

## Study of nonstandard interactions mediated by a scalar field at the ESSnuSB experiment

J. Aguilar,<sup>1</sup> M. Anastasopoulos,<sup>2</sup> E. Baussan,<sup>3</sup> A. K. Bhattacharyya,<sup>2</sup> A. Bignami,<sup>2</sup> M. Blennow,<sup>4,5</sup> M. Bogomilov,<sup>6</sup> B. Bolling,<sup>2</sup> E. Bouquerel,<sup>3</sup> F. Bramati,<sup>7</sup> A. Branca,<sup>7</sup> W. Brorsson,<sup>4,5,†</sup> G. Brunetti,<sup>7</sup> I. Bustinduy,<sup>1</sup> C. J. Carlile,<sup>8</sup> J. Cederkall,<sup>8</sup> T. W. Choi,<sup>9</sup> S. Choubey,<sup>4,5,‡</sup> P. Christiansen,<sup>8</sup> M. Collins,<sup>2,10</sup> E. Cristaldo Morales,<sup>7</sup> H. Danared,<sup>2</sup> D. Dancila,<sup>9</sup> J. P. A. M. de André,<sup>3</sup> M. Dracos,<sup>3</sup> I. Efthymiopoulos,<sup>11</sup> T. Ekelöf,<sup>9</sup> M. Eshraqi,<sup>2</sup> G. Fanourakis,<sup>12</sup> A. Farricker,<sup>13</sup> E. Fasoula,<sup>14,¶</sup> T. Fukuda,<sup>15</sup> N. Gazis,<sup>2</sup> Th. Gerasis,<sup>12</sup> M. Ghosh,<sup>16,§</sup> A. Giannetti,<sup>17</sup> G. Gokbulut,<sup>18,\*</sup> C. Hagner,<sup>19</sup> L. Halić,<sup>16</sup> V. T. Hariharan,<sup>19</sup> K. E. Iversen,<sup>8</sup> M. Jenssen,<sup>2</sup> R. Johansson,<sup>2</sup> E. Kasimi,<sup>14,¶</sup> A. Kayis Topaksu,<sup>18</sup> B. Kildetof,<sup>2</sup> B. Kliček,<sup>16</sup> K. Kordas,<sup>14,¶</sup> A. Leisos,<sup>14</sup> M. Lindroos,<sup>2,8,\*</sup> A. Longhin,<sup>20</sup> C. Maiano,<sup>2</sup> S. Marangoni,<sup>7</sup> C. Marrelli,<sup>2</sup> C. Martins,<sup>2</sup> D. Meloni,<sup>17</sup> M. Mezzetto,<sup>21</sup> N. Milas,<sup>2</sup> J. L. Muñoz,<sup>1</sup> M. Oglakci,<sup>18</sup> T. Ohlsson,<sup>4,5</sup> M. Ovegård,<sup>9</sup> M. Pari,<sup>20</sup> D. Patrzalek,<sup>2</sup> G. Petkov,<sup>6</sup> Ch. Petridou,<sup>14,¶</sup> P. Poussot,<sup>3</sup> A. Psallidas,<sup>12</sup> F. Pupilli,<sup>21</sup> D. Raikwal,<sup>22,23,||</sup> D. Saiang,<sup>24</sup> D. Sampsonidis,<sup>14,¶</sup> C. Schwab,<sup>3</sup> F. Sordo,<sup>1</sup> A. Sosa,<sup>2</sup> G. Stavropoulos,<sup>12</sup> M. Stipčević,<sup>16</sup> R. Tarkeshian,<sup>2</sup> F. Terranova,<sup>7</sup> T. Tolba,<sup>19</sup> E. Trachanas,<sup>2</sup> R. Tsenov,<sup>6</sup> A. Tsirigotis,<sup>14</sup> S. E. Tzamarias,<sup>14,¶</sup> G. Vankova-Kirilova,<sup>6</sup> N. Vassilopoulos,<sup>25</sup> S. Vihonen,<sup>4,5</sup> J. Wurtz,<sup>3</sup> V. Zeter,<sup>3</sup> O. Zormpa,<sup>12</sup> and Y. Zou<sup>9,††</sup>

(ESSnuSB Collaboration)

<sup>1</sup>*Consortio ESS-bilbao, Parque Científico y Tecnológico de Bizkaia, Laida Bidea, Edificio 207-B, 48160 Derio, Bizkaia*

<sup>2</sup>*European Spallation Source, Box 176, SE-221 00 Lund, Sweden*

<sup>3</sup>*IPHC, Université de Strasbourg, CNRS/IN2P3, F-67037 Strasbourg, France*

<sup>4</sup>*Department of Physics, School of Engineering Sciences, KTH Royal Institute of Technology, Roslagstullsbacken 21, 106 91 Stockholm, Sweden*

<sup>5</sup>*The Oskar Klein Centre, AlbaNova University Center, Roslagstullsbacken 21, 106 91 Stockholm, Sweden*

<sup>6</sup>*Faculty of Physics, Sofia University St. Kliment Ohridski, 1164 Sofia, Bulgaria*

<sup>7</sup>*University of Milano-Bicocca and INFN Sezione di Milano-Bicocca, 20126 Milano, Italy*

<sup>8</sup>*Department of Physics, Lund University, P.O. Box 118, 221 00 Lund, Sweden*

<sup>9</sup>*Department of Physics and Astronomy, FREIA Division, Uppsala University, P.O. Box 516, 751 20 Uppsala, Sweden*

<sup>10</sup>*Faculty of Engineering, Lund University, P.O. Box 118, 221 00 Lund, Sweden*

<sup>11</sup>*CERN, 1211 Geneva 23, Switzerland*

<sup>12</sup>*Institute of Nuclear and Particle Physics, NCSR Demokritos, Neapoleos 27, 15341 Agia Paraskevi, Greece*

<sup>13</sup>*Cockcroft Institute (A36), Liverpool University, Warrington WA4 4AD, United Kingdom*

<sup>14</sup>*Department of Physics, Aristotle University of Thessaloniki, Thessaloniki, Greece*

<sup>15</sup>*Institute for Advanced Research, Nagoya University, Nagoya 464–8601, Japan*

<sup>16</sup>*Center of Excellence for Advanced Materials and Sensing Devices, Ruđer Bošković Institute, 10000 Zagreb, Croatia*

<sup>17</sup>*Dipartimento di Matematica e Fisica, Università di Roma Tre, Via della Vasca Navale 84, 00146 Rome, Italy*

<sup>18</sup>*Department of Physics, Faculty of Science and Letters, University of Cukurova, 01330 Adana, Turkey*

<sup>19</sup>*Institute for Experimental Physics, Hamburg University, 22761 Hamburg, Germany*

<sup>20</sup>*Department of Physics and Astronomy “G. Galilei,” University of Padova and INFN Sezione di Padova, Padova, Italy*

<sup>21</sup>*INFN Sezione di Padova, Padova, Italy*

<sup>22</sup>*Harish-Chandra Research Institute, A CI of Homi Bhabha National Institute, Chhatnag Road, Jhansi, Prayagraj 211019, India*

<sup>23</sup>*Homi Bhabha National Institute, Anushakti Nagar, Mumbai 400094, India*

<sup>24</sup>*Department of Civil, Environmental, and Natural Resources Engineering, Luleå University of Technology, SE-971 87 Lulea, Sweden*

<sup>25</sup>*Institute of High Energy Physics (IHEP) Dongguan Campus, Chinese Academy of Sciences (CAS),  
1 Zhongzhiyuan Road, Dongguan, Guangdong 523803, China*



(Received 26 October 2023; accepted 26 April 2024; published 11 June 2024)

In this paper, we study scalar mediator induced nonstandard interactions (SNSIs) in the context of the ESSnuSB experiment. In particular, we study the capability of ESSnuSB to put bounds on the SNSI parameters and also study the impact of SNSIs in the measurement of the leptonic  $CP$  phase  $\delta_{CP}$ . Existence of SNSIs modifies the neutrino mass matrix and this modification can be expressed in terms of three diagonal real parameters ( $\eta_{ee}$ ,  $\eta_{\mu\mu}$ , and  $\eta_{\tau\tau}$ ) and three off-diagonal complex parameters ( $\eta_{e\mu}$ ,  $\eta_{e\tau}$ , and  $\eta_{\mu\tau}$ ). Our study shows that the upper bounds on the parameters  $\eta_{\mu\mu}$  and  $\eta_{\tau\tau}$  depend upon how  $\Delta m_{31}^2$  is minimized in the theory. However, this is not the case when one tries to measure the impact of SNSIs on  $\delta_{CP}$ . Further, we show that the  $CP$  sensitivity of ESSnuSB can be completely lost for certain values of  $\eta_{ee}$  and  $\eta_{\mu\tau}$  for which the appearance channel probability becomes independent of  $\delta_{CP}$ .

DOI: [10.1103/PhysRevD.109.115010](https://doi.org/10.1103/PhysRevD.109.115010)

## I. INTRODUCTION

In the standard three flavor model, the quantum mechanical interference phenomenon of neutrino oscillations can be described by three mixing angles  $\theta_{13}$ ,  $\theta_{23}$ ,  $\theta_{13}$ , two mass squared differences  $\Delta m_{21}^2$ ,  $\Delta m_{31}^2$ , and the Dirac type  $CP$  phase  $\delta_{CP}$ . Among these parameters, the true nature of  $\delta_{CP}$  is yet to be understood [1]. The currently running experiment T2K prefers a  $CP$  violating value of  $\delta_{CP}$ , whereas the data from the NOvA experiment are consistent with a  $CP$  conserving value of this parameter [2]. Therefore, the aim of the next generation of experiments will be to measure this parameter with significant precision. ESSnuSB [3] is an upcoming accelerator-based neutrino oscillation experiment that aims to measure  $\delta_{CP}$  by measuring the second oscillation maximum. Recently, the feasibility study of ESSnuSB was published in the conceptual design report (CDR) [4]. The proposal is to double the repetition rate and compress the beam pulses of the European spallation source (ESS) [5] to produce a 5 MW proton beam for neutrino production. The neutrinos produced in the ESS will be detected at a distance of 360 km using a megaton-scale underground water Cherenkov

neutrino detector. The CDR reports the required upgrades of the ESS linac, design of the target station, optimization of the near and far detectors, and the expected sensitivity to  $\delta_{CP}$ . Additionally, there is also a proposal [6] to build a low energy muon storage ring similar to the nuSTORM [7] project and to build a low energy monitored neutrino beam line, inspired by the ENUBET project [8].

The ESSnuSB experiment provides us with an opportunity to study various new physics scenarios beyond the standard three flavor model. One such scenario is non-standard interactions (NSIs). NSIs can be mediated either by a vector field or a scalar field. NSI mediated by a vector field can be either charged current (CC) in nature, which affects the neutrino interactions during their production and detection, or it can also be neutral current (NC) in nature affecting the neutrino propagation. In the context of ESSnuSB, CC NSI has been studied in Ref. [9], whereas NC NSI in ESSnuSB has been studied in Ref. [10]. However, it should be noted that, as the ESSnuSB is not very sensitive to matter effects, the changes in the neutrino oscillation probability due to NC NSI is negligible. This is because the presence of NC NSI alters the matter potential of the Hamiltonian. In this paper, we will study the effect of a different kind of NSI, which is mediated by a scalar field (i.e., SNSIs), in the context of the ESSnuSB experiment. In the presence of SNSI, the Lagrangian is extended by a Yukawa-like term and therefore its effect in the neutrino oscillation Hamiltonian appears as a correction to the neutrino mass. This new contribution to the neutrino mass term can be parametrized by  $\eta_{\alpha\beta}$ . Our aim in this work will be to study the capability of ESSnuSB to constrain the parameters of SNSI and to see how the  $\delta_{CP}$  sensitivity is affected if SNSI exists in nature. Recently, in Ref. [11], the sensitivity of ESSnuSB to SNSI was studied for  $\eta_{ee}$ . Note that the original aim of Ref. [11] was to study the interaction between an ultralight scalar field (ULSF) and active neutrinos in the context where the ULSF can act as a dark matter, whereas SNSI is basically an effective

\*Deceased.

†Corresponding author: wbro@kth.se

‡Corresponding author: choubey@kth.se

§Corresponding author: mghosh@irb.hr

||Corresponding author: deepakraikwal@hri.res.in

¶Also at Center for Interdisciplinary Research and Innovation (CIRI-AUTH), Thessaloniki, Greece.

\*\*Also at Department of Physics and Astronomy, Ghent University, Proeftuinststraat 86, 9000 Ghent, Belgium.

††Also at Advanced Light Source Research Center, Wuhan University, Wuhan, China.

*Published by the American Physical Society under the terms of the Creative Commons Attribution 4.0 International license. Further distribution of this work must maintain attribution to the author(s) and the published article's title, journal citation, and DOI. Funded by SCOAP<sup>3</sup>.*

interaction mediated by a heavy scalar field. However, the modification of the neutrino oscillation probabilities due to the ULSF parameter is similar to that of the modification of the neutrino oscillation probabilities due to SNSI. Therefore the results obtained in Ref. [11] can be directly compared with the results of SNSI. In that article, the authors showed how the upper bound of  $\eta_{ee}$  depends upon  $\theta_{23}$  and  $\Delta m_{31}^2$ . They found that the standard three flavor scenario and the SNSI scenario can be distinguished at  $3\sigma$  if  $\eta_{ee}$  is greater than 0.045 for the 360 km baseline of ESSnuSB. In our study, we extend the analysis for all six SNSI parameters (three real and three complex). Our results show that the upper bounds on the SNSI parameters  $\eta_{\mu\mu}$  and  $\eta_{\tau\tau}$  depend upon how the  $\chi^2$  is minimized with respect to the parameter  $\Delta m_{31}^2$ . While studying the effect of SNSI on the measurement of  $\delta_{CP}$ , we find that, for some values of the SNSI parameters  $\eta_{ee}$  and  $\eta_{\mu\tau}$ , the appearance channel probability becomes independent of  $\delta_{CP}$  and hence the  $\delta_{CP}$  sensitivity is completely lost. Regarding the study of SNSI for other experiments, we refer to Refs. [11–22].

The article is organized as follows. In the next section, we will provide the theoretical background of the SNSI. In Sec. III, we will provide the description of the configuration of the ESSnuSB experiment that we use in our calculations. In Sec. IV, we present our results. In the beginning of this section, we will provide the details of our simulation and then we divide it in two parts. In the first part, we will study the capability of ESSnuSB to put bounds on the SNSI parameters, and in the second part, we will study the impact of SNSI on the measurement of  $\delta_{CP}$  for ESSnuSB. Finally, in Sec. V, we will summarize our main findings and give our concluding remarks.

## II. NONSTANDARD INTERACTIONS MEDIATED BY SCALAR FIELD

The Lagrangian corresponding to the simplest model that describes SNSI can be written as [23]

$$\mathcal{L} = \bar{\nu}(i\gamma^\mu \partial_\mu - m_\nu)\nu - (y_\nu)_{\alpha\beta} \bar{\nu}_\alpha \nu_\beta \phi - (y_f)_{\alpha\beta} \bar{f}_\alpha f_\beta \phi - \frac{1}{2}(\partial_\mu \phi)^2 - \frac{m_\phi^2}{2}\phi^2, \quad (2.1)$$

where  $y_f$  is the Yukawa coupling of the scalar mediator  $\phi$  with fermion  $f$ ,  $y_\nu$  is the Yukawa coupling of the scalar mediator with the neutrinos  $\nu$ , and  $m_\phi$  is the mass of the scalar mediator. Here  $\alpha$  and  $\beta$  are the flavor indices of the leptons. Therefore, the effective Lagrangian in the presence of SNSI can be written as

$$\mathcal{L}_{\text{eff}} = \sum_{f,\alpha,\beta} \frac{y_f y_\nu}{m_\phi^2} (\bar{\nu}_\alpha \nu_\beta)(f\bar{f}), \quad (2.2)$$

From Eq. (2.1) we see that the effective Lagrangian is composed of Yukawa terms. Therefore, unlike the NSI

mediated by a vector field, SNSI will not appear as a contribution to the matter potential in the Hamiltonian; rather it can appear as a medium-dependent correction to the neutrino mass term. This correction to the neutrino mass matrix can be written as

$$\delta M = \frac{\sum_f N_f y_f y_\nu}{m_\phi^2}, \quad (2.3)$$

where  $N_f$  is the density of the fermion in matter. One convenient way to parametrize  $\delta M$  can be [12]

$$\delta M = \sqrt{|\Delta m_{31}^2|} \begin{pmatrix} \eta_{ee} & \eta_{e\mu} & \eta_{e\tau} \\ \eta_{\mu e} & \eta_{\mu\mu} & \eta_{\mu\tau} \\ \eta_{\tau e} & \eta_{\tau\mu} & \eta_{\tau\tau} \end{pmatrix}, \quad (2.4)$$

where we have chosen to scale the size of  $\delta M$  relative to  $\sqrt{|\Delta m_{31}^2|}$  to make the parameters of SNSI, i.e.,  $\eta$  dimensionless. This parametrization provides an easy comparison with the original mass term. Comparing Eqs. (2.3) and (2.4), one can write

$$\eta_{\alpha\beta} = \frac{1}{m_\phi^2 \sqrt{|\Delta m_{31}^2|}} \sum_f N_f y_f y_{\alpha\beta}. \quad (2.5)$$

We will consider  $\delta M$  to be Hermitian, hence,  $\eta_{\alpha\alpha}$  are real and  $\eta_{\alpha\beta} = \eta_{\beta\alpha}^* = |\eta_{\alpha\beta}| e^{i\phi_{\alpha\beta}}$  with  $\alpha \neq \beta$  are complex. Therefore, the number of real independent parameters is nine.

Here it is important to discuss the present bounds on the Yukawa couplings and the mass of the scalar mediator and how our results compare with these bounds. Our intention in this work is to estimate the sensitivity of ESSnuSB to the effective coupling  $\eta_{\alpha\beta}$  in a model-independent way. While the expressions given by Eqs. (2.1)–(2.5) in our manuscript assume one of the most well-motivated model scenarios that could give rise to such effective coupling at tree level, the bounds obtained in our analysis remain truly model independent. However, within the framework of a simple model with just one additional scalar, the effective couplings  $\eta_{\alpha\beta}$  receive constraints from several earlier experiments—both oscillation as well as nonoscillation experiments. The oscillation experiments put bounds on  $\eta_{\alpha\beta}$  via the oscillation probabilities in the same way as ESSnuSB and are totally model independent. Recently, such bounds have been calculated in the context of DUNE [23], P2SO [20], and JUNO [15]. We can also get bounds from experiments that are sensitive to neutrino-electron and/or neutrino-nucleon elastic scattering [24]. These bounds would also be expected to be model independent. The most stringent bound comes from XENONnT, which constrains  $\sqrt{y_\nu y_e} \simeq 8 \times 10^{-7}$  for  $m_\phi \simeq 10$  keV [25–27]. The COHERENT experiment puts a slightly weaker bound  $\sqrt{y_\nu y_e/N} \simeq 2 \times 10^{-5}$  for  $m_\phi \simeq 10$  MeV [23]. As discussed in Ref. [23], this scenario is expected to be constrained also

TABLE I. Oscillation parameters provided by NuFIT 5.2 (2022) (with Super-Kamiokande atmospheric data).

Parameter	Best fit $\pm 1\sigma$	$3\sigma$ range
$\sin^2 \theta_{12}$	$0.303 \pm 0.012$	
$\theta_{12}$	$0.583 \pm 0.013$	$0.546 \rightarrow 0.624$
$\sin^2 \theta_{13}$	$0.02225 \pm 0.00059$	
$\theta_{13}$	$0.1497 \pm 0.0019$	$0.1436 \rightarrow 0.1555$
$\sin^2 \theta_{23}$	$0.451 \pm 0.019$	
$\theta_{23}$	$0.737 \pm 0.019$	$0.693 \rightarrow 0.890$
$\delta_{CP}$	$4.05 \pm 0.63$	$2.51 \rightarrow 6.11$
$\Delta m_{12}^2$	$(7.41 \pm 0.21) \times 10^{-5} \text{ eV}^2$	$(6.82 \rightarrow 8.03) \times 10^{-5} \text{ eV}^2$
$\Delta m_{13}^2$	$(2.507 \pm 0.027) \times 10^{-3} \text{ eV}^2$	$(2.427 \rightarrow 2.590) \times 10^{-3} \text{ eV}^2$

from Borexino data on solar neutrinos and data from SN1987A.

Now let us see how this  $\delta M$  modifies the Hamiltonian of neutrino oscillations. The Hamiltonian of neutrino oscillations in the flavor basis and in the presence of scalar NSI can be written as

$$H = E_\nu + \frac{MM^\dagger}{2E_\nu} + V, \quad (2.6)$$

where  $E_\nu$  is the energy of the neutrinos and  $V = \text{diag}(\sqrt{2}G_F N_e, 0, 0)$  is the standard matter potential, where  $G_F$  is the Fermi constant and  $N_e$  is the electron number density. In this case, the term  $M$  becomes

$$M = U \text{diag}(m_1, m_2, m_3) U^\dagger + \delta M \quad (2.7)$$

$$= U \text{diag}\left(m_1, \sqrt{m_1^2 + \Delta m_{21}^2}, \sqrt{m_1^2 + \Delta m_{31}^2}\right) U^\dagger + \delta M, \quad (2.8)$$

where in Eq. (2.8) we have assumed normal ordering of the neutrino masses, i.e.,  $m_3 > m_2 > m_1$ .<sup>1</sup> In the above equation,  $U$  is the Pontecorvo-Maki-Nakagawa-Sakata matrix. In our calculation, we used the standard parametrization of  $U$  as given in Ref. [28]. Neutrino oscillation probabilities in the presence of SNSI can be calculated by diagonalizing Eq. (2.6). Here it is interesting to note that, for SNSI, the neutrino oscillation probabilities will depend on the absolute neutrino mass  $m_1$ .

### III. EXPERIMENTAL AND SIMULATION DETAILS

We have used the GLOBES [29,30] software for our numerical calculations. In order to calculate the neutrino

<sup>1</sup>For the inverted ordering of the neutrino masses, i.e.,  $m_2 > m_1 > m_3$ , Eq. (2.8) can be written as  $M = U \text{diag}\left(\sqrt{m_3^2 + \Delta m_{31}^2}, \sqrt{m_3^2 + \Delta m_{21}^2 + \Delta m_{31}^2}, m_3\right) U^\dagger + \delta M$ . In this case, probabilities will depend on the absolute mass  $m_3$ .

oscillation probabilities in the presence of SNSI, we have modified the probability engine in GLOBES. For ESSnuSB we have used the exact configuration that is used to generate the results in the CDR [4]. A water Cherenkov detector of fiducial volume 538 kt located at a distance 360 km from the neutrino source has been considered. A value of  $2.7 \times 10^{23}$  protons on target/yr with a beam power of 5 MW and proton kinetic energy of 2.5 GeV has been assumed for the neutrino beam production. The optimized fluxes from the genetic algorithm have been implemented, together with the event selection obtained from the full Monte Carlo simulations in the form of migration matrices. The events are distributed in 50 bins between 0 and 2.5 GeV of the reconstructed energy. Both the appearance channel ( $\nu_\mu \rightarrow \nu_e$ ) and disappearance channel ( $\nu_\mu \rightarrow \nu_\mu$ ) for signal events have been analyzed. The relevant background channels have been implemented. Finally, a total run time of ten years (divided into five years of neutrino beam and five years of antineutrino beam) has been assumed. For systematics, we have considered an overall normalization error of 5% for signal and 10% for backgrounds for both appearance and disappearance channels. We did not consider any systematic errors corresponding to shape. This is because, in the ESSnuSB conceptual design report [4], it was shown that the effect of systematic uncertainty due to shape has very small effect on the  $\delta_{CP}$  sensitivity. Therefore, we do not expect that these uncertainties will have significant impact for the study of SNSI in ESSnuSB.

### IV. RESULTS

For the estimation of the sensitivity, we use the Poisson log-likelihood and assume that it is  $\chi^2$  distributed,

$$\chi_{\text{stat}}^2 = 2 \sum_{i=1}^n \left[ N_i^{\text{test}} - N_i^{\text{true}} - N_i^{\text{true}} \log \left( \frac{N_i^{\text{test}}}{N_i^{\text{true}}} \right) \right], \quad (4.1)$$

where  $N_i^{\text{test}}$  and  $N_i^{\text{true}}$  are the number of events in the test and true spectra, respectively, and  $n$  is the number of energy bins. The systematic error is incorporated by the method of

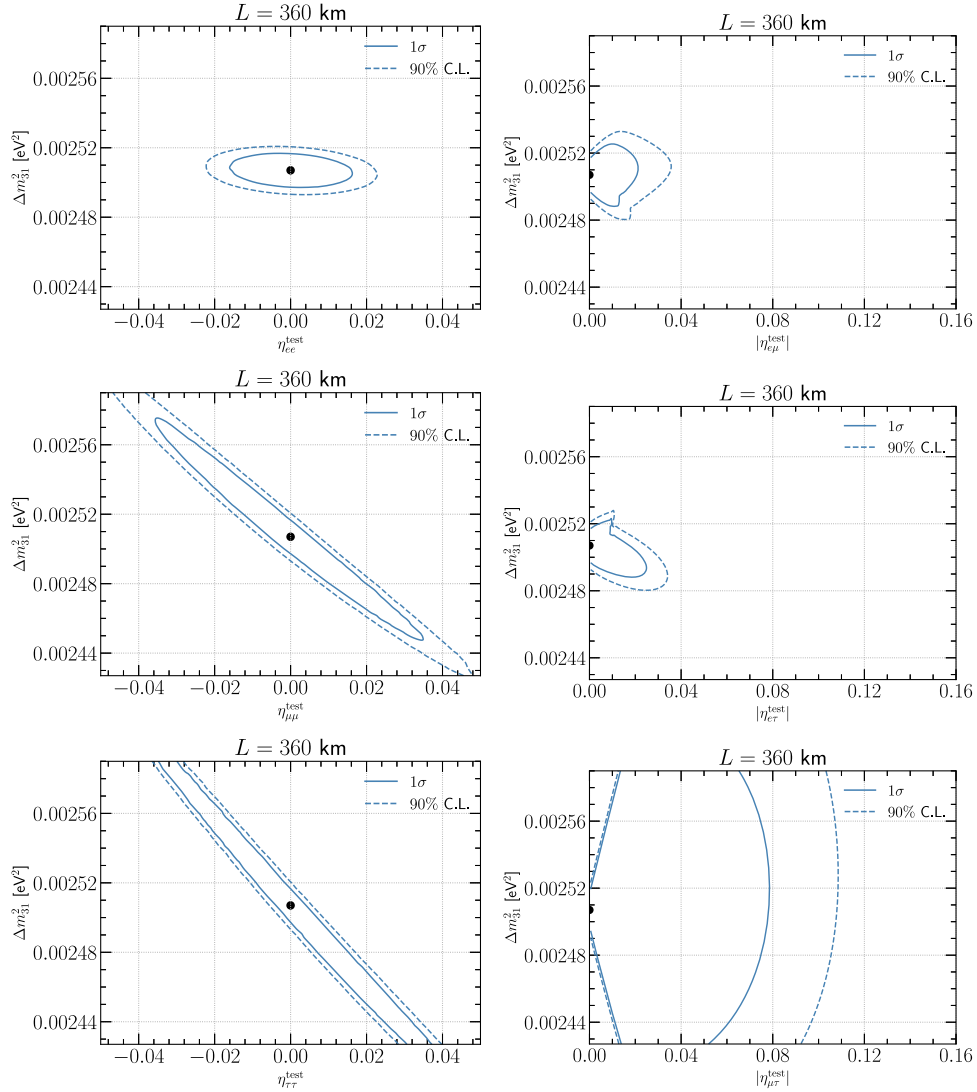


FIG. 1. 2D contours in the  $\eta$  (test)– $\Delta m_{31}^2$  (test) plane. In these panels,  $1\sigma$  (90% C.L.) contours correspond to  $\chi^2 = 2.30(4.61)$ . See text for details.

pull [31,32]. The values of the oscillation parameters are taken from NuFIT 5.2 and are listed in Table I.

While calculating the  $\chi^2$ , the true values of the oscillation parameters are always kept at their best-fit values as shown in Table I. Unless otherwise mentioned, the relevant oscillation parameters are minimized in the test using the current uncertainties associated with these parameters and all our results are presented for the normal ordering of the neutrino masses with  $m_1 = 7.42 \times 10^{-5} \text{ eV}^2$ . Further, we will consider one SNSI parameter at a time throughout our calculation.

### A. Bounds on the SNSI parameters

Let us first discuss the capability of ESSnuSB to put bounds on the SNSI parameters. We will do this by taking the standard three flavor scenario in the true spectrum of the  $\chi^2$  and the SNSI scenario in the test spectrum of the  $\chi^2$ . And

then we will show the results as 1D  $\chi^2$  for the diagonal SNSI parameters (i.e.,  $\chi^2$  vs  $\eta_{\alpha\alpha}$  plots) and as 2D contours for the off-diagonal SNSI parameters ( $\eta_{\alpha\beta}$  vs  $\phi_{\alpha\beta}$  plots with  $\alpha \neq \beta$ ). Before we present these results, it is important to understand how the bounds on the NSI parameters depend on the oscillation parameters. In our analysis, we have found that the parameter  $\Delta m_{31}^2$  has a very nontrivial role when putting the bounds on the SNSI parameters. In Fig. 1, we have taken the standard scenario in the true spectrum and SNSI in the test spectrum and plotted the 2D contours in the  $\eta$  vs  $\Delta m_{31}^2$  plane for  $1\sigma$  C.L. (solid contours) and 90% C.L. (dashed contours). In generating these plots, the parameter  $\theta_{23}$  is minimized using its  $1\sigma$  error as prior. The phases, i.e.,  $\delta_{CP}$  for all six panels and  $\phi$  for the off-diagonal parameters, are minimized without any prior, i.e., flat prior. The mass ordering has been assumed to be known. The left column is for the diagonal SNSI parameters with top/middle/bottom

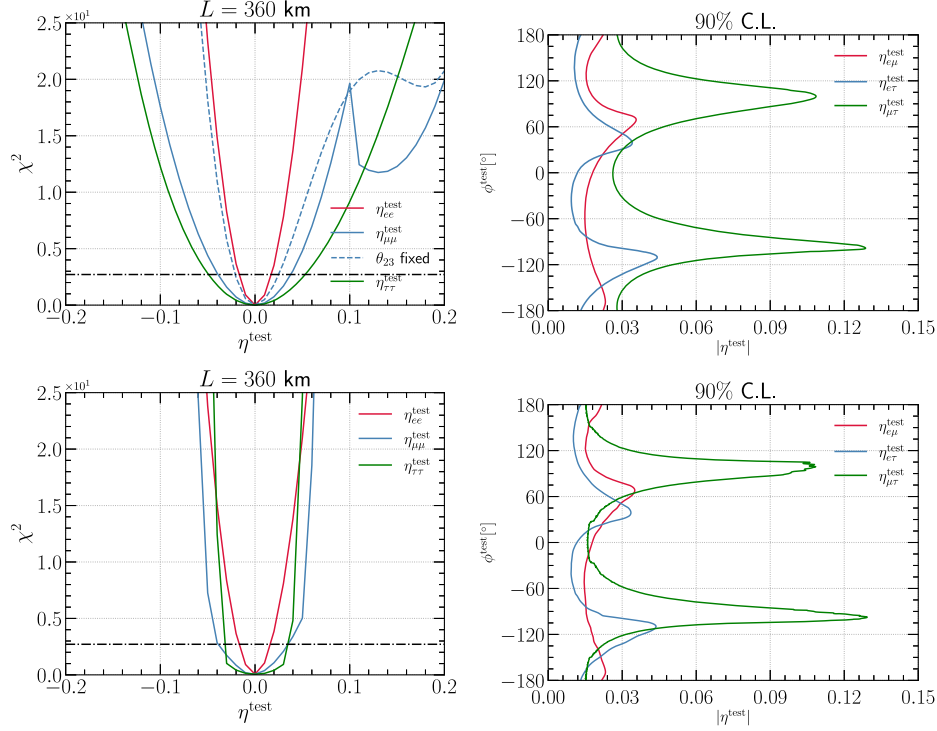


FIG. 2. Capability of ESSnuSB to put bounds on the SNSI parameters. Top row:  $\Delta m_{31}^2$  is minimized randomly without any prior. Bottom row:  $\Delta m_{31}^2$  is minimized within its current  $3\sigma$  values. See text for details.

panels corresponding to  $\eta_{ee}/\eta_{\mu\mu}/\eta_{\tau\tau}$ , whereas the right column is for the off-diagonal parameters with top/middle/bottom panels corresponding to  $\eta_{e\mu}/\eta_{e\tau}/\eta_{\mu\tau}$ . In these panels, the y axis corresponds to the current  $3\sigma$  allowed values of  $\Delta m_{31}^2$  according to NuFIT5.2.

From Fig. 1, we see that for the SNSI parameters  $\eta_{ee}$ ,  $\eta_{e\mu}$ , and  $\eta_{e\tau}$ , one obtains closed contours at both  $1\sigma$  and 90% C.L., i.e., within the  $3\sigma$  range of  $\Delta m_{31}^2$ . This implies that for these parameters the standard three flavor scenario can be fitted with SNSI with a value of  $\Delta m_{31}^2$  lying within its current  $3\sigma$  allowed values. However, this is not the case for the parameters  $\eta_{\mu\mu}$ ,  $\eta_{\tau\tau}$ , and  $\eta_{\mu\tau}$ . Here we notice that the contours at the 90% C.L. reach beyond the current  $3\sigma$  allowed values of  $\Delta m_{31}^2$ . This means that, for these parameters, the standard scenario can be fitted with SNSI with a value of  $\Delta m_{31}^2$  lying beyond its current  $3\sigma$  allowed values. This brings us to an important conclusion: that the bounds of the SNSI parameters  $\eta_{\mu\mu}$ ,  $\eta_{\tau\tau}$ , and  $\eta_{\mu\tau}$  can depend upon how  $\Delta m_{31}^2$  is minimized during the fit. If one minimizes  $\Delta m_{31}^2$  within its  $3\sigma$  values, then we will obtain stronger bounds as compared to the case when we minimize this parameter randomly without any prior. As in the later case, the  $\chi^2$  minimum can occur with a value of  $\Delta m_{31}^2$  lying outside its current  $3\sigma$  allowed values. This can be seen from Fig. 2.

In Fig. 2, we have shown the capability of ESSnuSB to put bounds on the SNSI parameters. The top row shows the

case when  $\Delta m_{31}^2$  is minimized randomly without any prior, i.e., flat prior, and the bottom row reflects the case when  $\Delta m_{31}^2$  is minimized within its  $3\sigma$  allowed values by the method of systematic sampling. By systematic sampling, we mean that the  $\chi^2$  is calculated by varying  $\Delta m_{31}^2$  in equidistant steps from its  $3\sigma$  minimum value to its  $3\sigma$  maximum value and then we select the  $\chi^2$  minimum. In each row, the left panels are for the diagonal parameters with red/blue/green curves corresponding to  $\eta_{ee}/\eta_{\mu\mu}/\eta_{\tau\tau}$ , whereas the right panels are for the off-diagonal parameters with red/blue/green curves corresponding to  $\eta_{e\mu}/\eta_{e\tau}/\eta_{\mu\tau}$ . In the left column, the black dash-dotted horizontal line shows the benchmark sensitivity of 90% C.L., whereas the right column shows the contours are drawn at 90% C.L.

From Fig. 2, we see that the curves for  $\eta_{ee}$ ,  $\eta_{e\mu}$ , and  $\eta_{e\tau}$  are very similar in the top and bottom rows, i.e., the sensitivity is very similar between the cases when  $\Delta m_{31}^2$  varies randomly without any prior vs when  $\Delta m_{31}^2$  is minimized within its  $3\sigma$  range. This is because, for these parameters, in both cases the  $\chi^2$  minimum appears with  $\Delta m_{31}^2$  lying within its current  $3\sigma$  values. However, this is not the case for the SNSI parameters  $\eta_{\mu\mu}$  and  $\eta_{\tau\tau}$ . For these parameters, the upper bounds obtained from the top row (for example, at  $3\sigma$  C.L.) are weaker as compared to the bounds that are obtained from the bottom row. This is because, in the bottom row, the  $\chi^2$  minimum is forced to occur within the current  $3\sigma$  values of  $\Delta m_{31}^2$ , whereas in the

TABLE II. Upper bounds of the SNSI parameters at  $3\sigma$  C.L. See text for details. In this table, 90% C.L. bounds for the diagonal (off-diagonal) SNSI parameters correspond to  $\chi^2 = 2.71(4.61)$ .

SNSI parameter	$\Delta m_{31}^2$ free		$\Delta m_{31}^2$ constrained	
	90% C.L. range	Phase	90% C.L. range	Phase
$\eta_{ee}$	$-0.01 \rightarrow 0.01$		$-0.01 \rightarrow 0.01$	
$\eta_{\mu\mu}$	$-0.04 \rightarrow 0.04$		$-0.04 \rightarrow 0.03$	
$\eta_{\tau\tau}$	$-0.05 \rightarrow 0.05$		$-0.0 \rightarrow 0.03$	
$ \eta_{e\mu} $	$0.000 \rightarrow 0.36$	$\phi_{e\mu} = 75^\circ$	$0.000 \rightarrow 0.036$	$\phi_{e\mu} = 75^\circ$
$ \eta_{e\tau} $	$0.000 \rightarrow 0.042$	$\phi_{e\tau} = -105^\circ$	$0.000 \rightarrow 0.042$	$\phi_{e\tau} = -105^\circ$
$ \eta_{\mu\tau} $	$0.000 \rightarrow 0.132$	$\phi_{\mu\tau} = -90^\circ$	$0.000 \rightarrow 0.132$	$\phi_{\mu\tau} = -90^\circ$

top row, where the  $\Delta m_{31}^2$  has been kept free, the  $\chi^2$  minimum occurs at a value of  $\Delta m_{31}^2$ , which lies outside its current  $3\sigma$  values. For  $\eta_{\mu\tau}$ , we see that the upper bounds for both cases are similar, though the standard scenario can be fitted with SNSI with a value of  $\Delta m_{31}^2$  lying beyond its current  $3\sigma$  allowed values. We have listed the 90% bounds obtained for the SNSI parameters in Table II for both cases.

In Fig. 2 (top left panel) we see a dip in the  $\eta_{\mu\mu}$  curve around 0.1. To understand this behavior, we have plotted the dashed curve where we keep the parameter  $\theta_{23}$  fixed to its best-fit value in the test spectrum of the  $\chi^2$ . As a result,

we see that the dip is mostly vanished. From this we conclude that the higher positive values of  $\eta_{\mu\mu}$  suffer from degeneracy with the standard oscillation parameters when the  $\chi^2$  is minimized without any constraints on  $\Delta m_{31}^2$ .

From Fig. 2, we see that, for the off-diagonal parameters, the upper bounds depend on the values of the phases  $\phi$ . For all three off-diagonal parameters, the strongest bound corresponds to  $\phi = 0^\circ$ . For  $\eta_{e\mu}$  the bound is weakest around  $\phi_{e\mu} = 90^\circ$ , whereas for  $\eta_{e\tau}$  and  $\eta_{\mu\tau}$ , the weakest bound comes around  $\phi_{e\mu} = -90^\circ$ . To understand this, we have plotted in Fig. 3 the appearance channel probabilities,

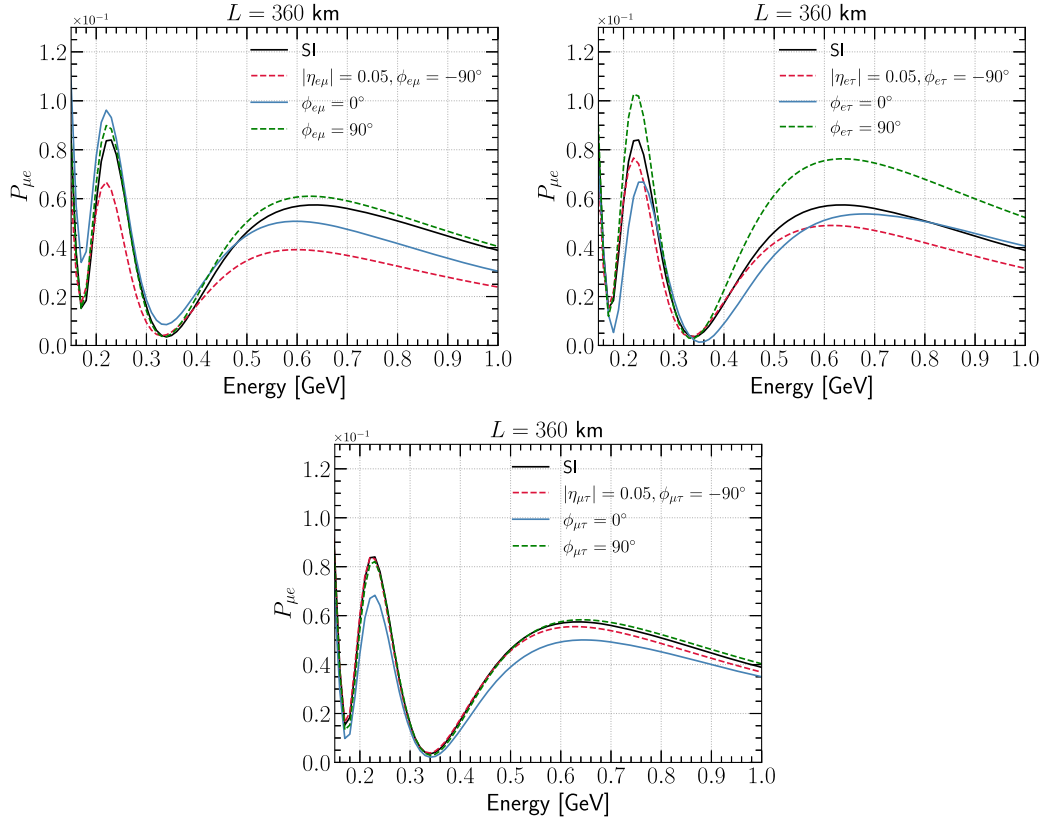


FIG. 3. Appearance channel probabilities as a function of  $E$  for the three off-diagonal SNSI parameters. The standard curve (SI) is drawn with the true values of oscillation parameters that are used to generate Fig. 2. The SNSI curves are drawn with the value of oscillation parameters, where the  $\chi^2$  minimum comes in the top row of Fig. 2.

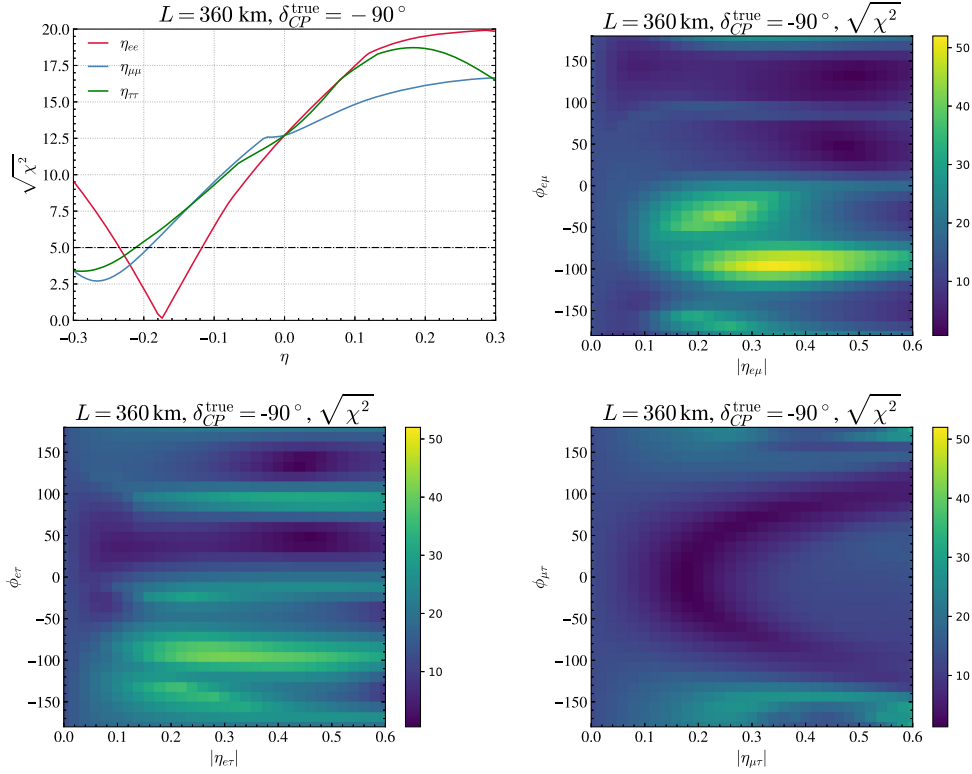


FIG. 4.  $CP$  violation discovery sensitivity for  $\delta_{CP}(\text{true}) = -90^\circ$  as function of the SNSI parameters.  $5\sigma$  is at  $\sqrt{\chi^2} = 5$ . See text for detail.

i.e.,  $P_{\mu e}$  for the neutrinos as a function of the energy for the 360 km baseline. The top left/top right/bottom panels are for  $\eta_{e\mu}/\eta_{e\tau}/\eta_{\mu\tau}$ . In each panel, the standard three flavor scenario is shown by the black solid curve. The values of the oscillation parameters for this curve are the same as the true values that are used to generate Fig. 2. The red, blue, and green curves correspond to the SNSI cases with  $\phi = -90^\circ, 0^\circ$ , and  $90^\circ$ , respectively. The values of  $|\eta|$  are taken to be 0.05 for all cases. The SNSI curves are drawn for the values of the oscillation parameters at which the  $\chi^2$  minimum occurs for the case when the  $\Delta m_{31}^2$  is minimized freely, i.e., the top row of Fig. 2. Therefore, the separation between the standard curve and the SNSI curves reflects the sensitivity of the SNSI parameters at that value of  $\phi$ . If the separation between the standard curve and the SNSI curve for a given value of  $\phi$  is large, then this would imply a stronger bound on the SNSI parameter for that value of  $\phi$ , whereas if the separation between the standard curve and SNSI curves is small, then we expect a weaker bound for the value of  $\phi$ . Further, as the flux  $\times$  cross section peaks around 0.35 GeV for ESSnuSB, we will be interested in the separation between the standard curves and SNSI curves around that value of  $E$ .

From the probability curves, we see that, for all three off-diagonal parameters, the black curve and the blue curves are separated the most. For this reason, we have observed that the strongest bound on the off-diagonal parameters

comes at  $\phi = 0^\circ$ . For  $\eta_{e\mu}$ , we see that the black curve and the green curve are the closest. This explains why the sensitivity is weak at  $\phi_{e\mu} = 90^\circ$ . For  $\eta_{e\tau}$  and  $\eta_{\mu\tau}$ , we notice that the black curve is closest to the red curve. This is why for these two parameters the weakest sensitivity comes around the  $-90^\circ$  value of the phases.<sup>2</sup>

### B. Impact of SNSI in the measurement of $\delta_{CP}$

In this subsection, we will discuss the effect of SNSI on the  $\delta_{CP}$  sensitivity of ESSnuSB assuming SNSI exists in nature. This is done by taking SNSI in both the true and test spectrum of the  $\chi^2$ . Like earlier, first we checked the effect of different oscillation parameters when one considers SNSI in both the true and test spectrum of the  $\chi^2$ . Here we have found that when SNSI is considered in both the true and test, the  $\chi^2$  minimum always appears within the current  $3\sigma$  allowed values of all parameters. Therefore, the sensitivity does not differ in the different cases depending upon how the different oscillation parameters are minimized.

In Fig. 4, we have shown the  $CP$  violation ( $CPV$ ) sensitivity for  $\delta_{CP}(\text{true}) = -90^\circ$  as a function of the SNSI parameters. The  $CPV$  discovery sensitivity of an

<sup>2</sup>For  $\eta_{e\tau}$  and  $\eta_{\mu\tau}$ , the black curve is also very close to the green curve, implying a weaker sensitivity around  $90^\circ$  at  $\eta = 0.05$  as seen in Fig. 2.

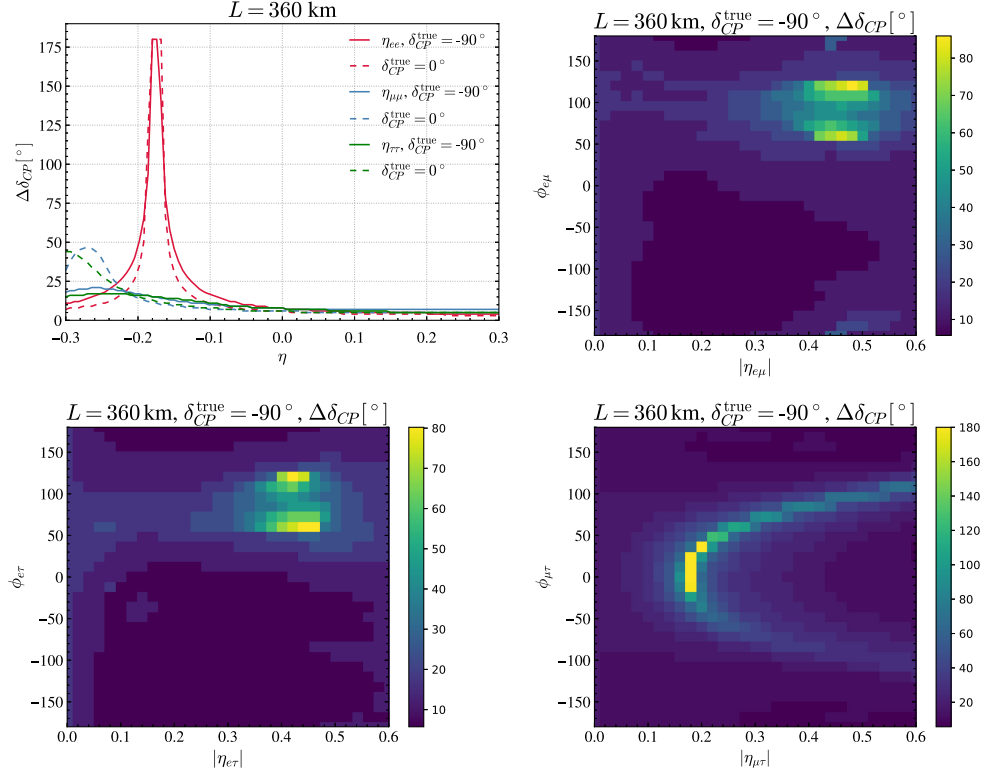


FIG. 5.  $CP$  precision sensitivity as function of the SNSI parameters. Here  $\Delta\delta_{CP}$  corresponds to the  $1\sigma$  error associated with  $\delta_{CP}$  corresponding to  $\chi^2 = 1$ . See text for details.

experiment is defined by its capability to distinguish a value of  $\delta_{CP}$  from non- $CPV$  values of  $0^\circ$  and  $180^\circ$ . The top left panel is for the diagonal parameters, whereas the other panels are for the off-diagonal parameters. For the diagonal parameters, we have plotted the sensitivity as a function of  $\eta$ , whereas for the off-diagonal parameters we have plotted the sensitivity as 2D color maps in the  $|\eta| - \phi$  plane. In the 2D color maps, the color code shows the value of the  $CP$  violation discovery  $\chi^2$ . For the diagonal parameters, red/blue/green curves correspond to  $\eta_{ee}/\eta_{\mu\mu}/\eta_{\tau\tau}$ . In the top left panel, the black dashed dotted horizontal line shows the benchmark sensitivity of  $5\sigma$ . In Fig. 4, the SNSI parameters are fixed in the test as true.

Let us first discuss the sensitivity for the diagonal SNSI parameters. From the top left panel of Fig. 4, we see that starting from  $\eta_{\alpha\alpha} = 0$ , as we decrease (increase) the value of  $\eta_{\alpha\alpha}$ , the sensitivity decreases (increases) as compared to the sensitivity in the standard three flavor scenario. However, the sensitivity eventually reaches a minimum (maximum) and thereafter increases (decreases). Here we observe an interesting feature for  $\eta_{ee}$ . For  $\eta_{ee}$ , around  $-0.176$ , the  $CPV$  sensitivity becomes almost zero. For the off-diagonal parameters, we also see that for some combinations of  $\eta$  and  $\phi$ , the  $CPV$  sensitivity can become very small. In fact, for  $(|\eta_{\mu\tau}| = 0.18, \phi_{\mu\tau} = 12^\circ)$ ,  $CPV$  sensitivity completely vanishes. This will be more clear from Fig. 5.

Next, let us discuss the effect of SNSI on the  $CP$  precision. In Fig. 5, we have plotted the  $1\sigma$   $CP$  precision as a function of the SNSI parameters. The  $CP$  precision is defined as the error associated with the measurement of  $\delta_{CP}$ . The top left panel is for the diagonal parameters, whereas the other panels are for the off-diagonal parameters. For the diagonal parameters, we have plotted the sensitivity as a function of  $\eta$  for  $\delta_{CP} = 0^\circ$  and  $-90^\circ$ , whereas for the off-diagonal parameters we have plotted the sensitivity as 2D color maps in the  $|\eta| - \phi$  plane. Here the color code shows the  $1\sigma$  error associated with the measurement of  $\delta_{CP} = -90^\circ$ . For the diagonal parameters, red/blue/green curves correspond to  $\eta_{ee}/\eta_{\mu\mu}/\eta_{\tau\tau}$ . The solid (dashed) lines are for  $\delta_{CP} = -90^\circ$  ( $0^\circ$ ). In these panels, the SNSI parameters are fixed in the test as true.

For the diagonal parameters, we see that for the positive values of  $\eta$ , the sensitivity almost remains constant, whereas for the negative values of  $\eta$ , the sensitivity decreases as compared to the sensitivity in the standard three flavor scenario. Here also we see that for  $\eta_{ee}$ , around  $-0.176$ , the sensitivity is completely lost. We also see a similar effect for the off-diagonal parameters where the  $CP$  precision is very poor for some combination of  $\eta$  and  $\phi$ . For example, we can see that the  $CP$  precision sensitivity is completely lost for  $(|\eta_{\mu\tau}| = 0.18, \phi_{\mu\tau} = 12^\circ)$  (the yellow squares).

To understand why the  $CP$  sensitivity is completely lost for some values of the SNSI parameters, in Fig. 6 we have

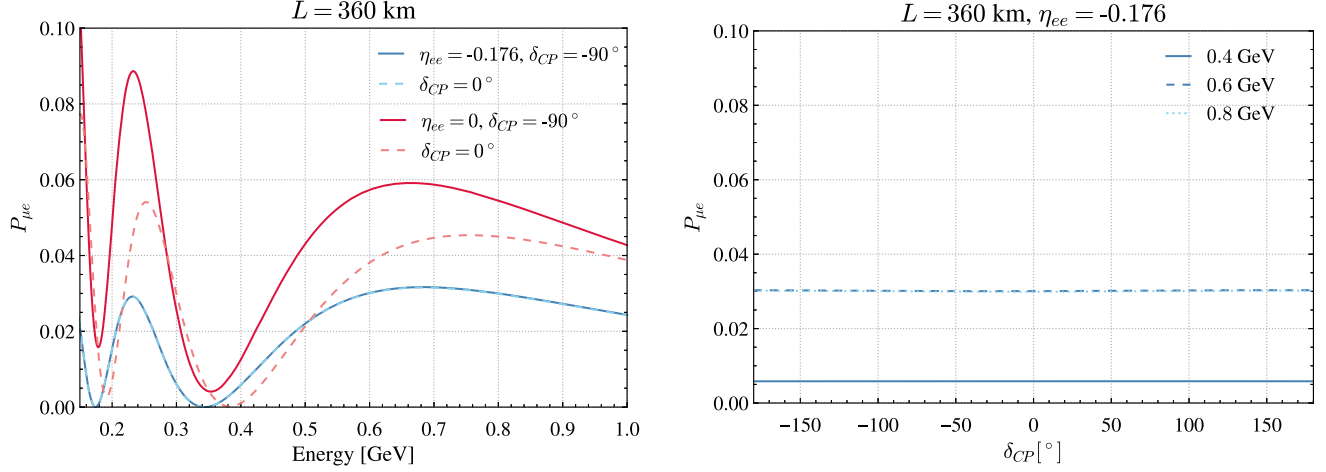


FIG. 6. Appearance channel probability as a function of energy (left) and the same as a function of  $\delta_{CP}$  (right). See text for details.

plotted the appearance channel probability for  $\eta_{ee} = -0.176$ . In the left panel, we have plotted the probability as a function of energy  $E$  for different values of  $\delta_{CP}$  and in the right panel we have plotted the probability as a function of  $\delta_{CP}$  for different values of  $E$ . In the left panel, the red curves are for the standard three flavor case and the blue is for the SNSI case.

From Fig. 6 (left panel), we see that for  $\eta_{ee} = -0.176$ , the curves for  $\delta_{CP} = -90^\circ$  and  $0^\circ$  are exactly overlapping for all values of  $E$ , whereas from the right panel we see that curves for different  $E$  are almost flat with respect to different values of  $\delta_{CP}$ . From this observation we can conclude that, for this particular value of  $\eta_{ee}$ , the appearance channel probability becomes independent of the  $\delta_{CP}$  and therefore the  $CP$  sensitivity is completely lost. This has been also shown in Ref. [20], where the authors have derived an analytical expression of the appearance channel probability for  $\eta_{ee}$ . In that article, the authors have analytically shown that the  $\delta_{CP}$ -dependent term in the probability becomes zero for  $\eta_{ee}$  around  $-0.17$ . A similar conclusion can be drawn about the loss of sensitivity for ( $|\eta_{\mu\tau}| = 0.18, \phi_{\mu\tau} = 12^\circ$ ).

## V. SUMMARY AND CONCLUSION

In this paper, we have studied the scalar mediator induced nonstandard interactions in the context of the ESSnuSB experiment. ESSnuSB is a future neutrino experiment that aims toward an unprecedented precision measurement of the leptonic  $CP$  phase  $\delta_{CP}$  by studying the phenomenon of neutrino oscillation at the second oscillation maximum. Apart from the oscillation in the standard three flavor scenario, ESSnuSB provides us with an opportunity to study various new physics scenarios. One of them is SNSI. In the presence of SNSI, the neutrino mass matrix gets modified. This modification can be parametrized in terms of three real diagonal parameters and three

complex off-diagonal parameters. In this work, we studied the capability of the ESSnuSB experiment to put the limit on the SNSI parameters as well as the impact of SNSI in the measurement of  $\delta_{CP}$ . We also looked at the impact of SNSI to the  $CP$  violation sensitivity of ESSnuSB.

To estimate the upper bounds on the SNSI parameters in the context of ESSnuSB, we took the standard three flavor model in the true spectrum of the  $\chi^2$  and SNSI in the test spectrum of the  $\chi^2$ . In our calculation we found that the parameter  $\Delta m_{31}^2$  plays a nontrivial role. The upper bounds on the parameters  $\eta_{\mu\mu}$ ,  $\eta_{\tau\tau}$ , and  $\eta_{\mu\tau}$  can depend upon how  $\Delta m_{31}^2$  is minimized in the theory. We showed that this happens because, for these parameters, the standard scenario can be fitted with SNSI with a value of  $\Delta m_{31}^2$  lying outside its current  $3\sigma$  allowed range. Therefore, if one minimizes this parameter within its current  $3\sigma$  range, then one will get a stronger bound on these parameters as compared to the case when one minimizes these parameters without any constraint. However, this is not the case with the other SNSI parameters, i.e.,  $\eta_{ee}$ ,  $\eta_{e\mu}$ , and  $\eta_{e\tau}$ . For them, the standard scenario can be always fitted with SNSI with a value of  $\Delta m_{31}^2$  lying within its current  $3\sigma$  values. In our analysis, we also find that the upper bounds of  $\eta_{\mu\tau}$  do not depend upon the minimization method of  $\Delta m_{31}^2$ , though the standard scenario can be fitted with SNSI with a value of  $\Delta m_{31}^2$  lying beyond its current  $3\sigma$  allowed values. We presented the sensitivity of ESSnuSB to  $\eta_{\alpha\beta}$  with and without the  $\Delta m_{31}^2$  constraints.

Next, we studied the impact of SNSI in the measurement of  $\delta_{CP}$  by taking SNSI in both the true and test spectrum of the  $\chi^2$ . Here we found that when one considers SNSI in both the true and test spectrum of the  $\chi^2$ , the results do not depend upon how the oscillation parameters are minimized in the test. In our study, we found that the  $CP$  sensitivity in terms of both  $CP$  violation and  $CP$  precision can either increase or decrease as compared to the sensitivity in the

standard three flavor case, depending upon the values of the SNSI parameters. Interestingly, we found that, for some values of the SNSI parameters, the  $CP$  sensitivity can become extremely poor. In particular, for  $\eta_{ee} = -0.176$  and ( $|\eta_{\mu\tau}| = 0.18$ ,  $\phi_{\mu\tau} = 12^\circ$ ) the appearance channel probability becomes independent of  $\delta_{CP}$  and hence the  $CP$  sensitivity of ESSnuSB is completely lost.

Note that in this study we have presented our results assuming the normal ordering of the neutrino masses. In principle, one should also investigate the case for the inverted ordering of the neutrino masses. In particular, it will be interesting to study if the degeneracies associated with the parameters  $\Delta m_{31}^2$  and  $\delta_{CP}$  manifest similarly for the inverted ordering. However, as the present data show a preference toward the normal ordering [1], we do not explore this in our present study.

In conclusion, the presence of SNSI can alter our understanding of neutrino oscillation in the three flavor scenario completely. It can affect the measurement of  $\Delta m_{31}^2$  and  $\delta_{CP}$  in a very significant manner. Therefore, it is very important to analyze the data from neutrino oscillation experiments to look for existence of SNSI. The ESSnuSB experiment provides a promising platform for studying SNSI.

## ACKNOWLEDGMENTS

We would like to thank Dinesh Kumar Singha for useful discussion. Funded by the European Union. Views and opinions expressed are however those of the author(s) only and do not necessarily reflect those of the European Union. Neither the European Union nor the granting authority can be held responsible for them. We acknowledge further support provided by the following research funding agencies: Centre National de la Recherche Scientifique, France; the Excellence Strategy of the Federal Government and the Länder, Germany; Ministry of Science and Education of Republic of Croatia Grant No. KK.01.1.1.01.0001; the Swedish Research Council (Vetenskapsrådet) through Contract No. 2017-03934; the European Union's Horizon 2020 research and innovation program under the Marie Skłodowska-Curie Grant Agreement No. 860881-HIDDeN; the European Union NextGenerationEU, through the National Recovery and Resilience Plan of the Republic of Bulgaria, Project No. BG-RRP-2.004-0008-C01; as well as support provided by the universities and laboratories to which the authors of this report are affiliated, see the author list on the first page.

- 
- [1] I. Esteban, M. C. Gonzalez-Garcia, M. Maltoni, T. Schwetz, and A. Zhou, The fate of hints: Updated global analysis of three-flavor neutrino oscillations, *J. High Energy Phys.* **09** (2020) 178.
  - [2] M. A. Ramírez *et al.* (T2K Collaboration), Measurements of neutrino oscillation parameters from the T2K experiment using  $3.6 \times 10^{21}$  protons on target, *Eur. Phys. J. C* **83**, 782 (2023).
  - [3] A. Alekou *et al.* (ESSnuSB Collaboration), Updated physics performance of the ESSnuSB experiment: ESSnuSB Collaboration, *Eur. Phys. J. C* **81**, 1130 (2021).
  - [4] A. Alekou *et al.*, The European Spallation Source neutrino super-beam conceptual design report, *Eur. Phys. J. Special Topics* **231**, 3779 (2022).
  - [5] H. Abele *et al.*, Particle physics at the European Spallation Source, *Phys. Rep.* **1023**, 1 (2023).
  - [6] A. Alekou *et al.*, The ESSnuSB design study: Overview and future prospects, *Universe* **9**, 347 (2023).
  - [7] L. A. Ruso *et al.* (nuSTORM Collaboration), Neutrinos from stored muons (nuSTORM), in *Snowmass 2021* (2022), p. 3; [arXiv:2203.07545](https://arxiv.org/abs/2203.07545).
  - [8] A. Longhin and F. Terranova (ENUBET Collaboration), Enhanced neutrino beams from kaon tagging (ENUBET), [arXiv:2203.08319](https://arxiv.org/abs/2203.08319).
  - [9] M. Blennow, S. Choubey, T. Ohlsson, and S. K. Raut, Exploring source and detector non-standard neutrino interactions at ESSnuSB, *J. High Energy Phys.* **09** (2015) 096.
  - [10] L. A. Delgadillo and O. G. Miranda, Future leptonic  $CP$  phase determination in the presence of NSI, *Phys. Rev. D* **108**, 095024 (2023).
  - [11] R. Cordero, L. A. Delgadillo, and O. G. Miranda, European Spallation Source as a searching tool for an ultralight scalar field, *Phys. Rev. D* **107**, 075023 (2023).
  - [12] S.-F. Ge and S. J. Parke, Scalar nonstandard interactions in neutrino oscillation, *Phys. Rev. Lett.* **122**, 211801 (2019).
  - [13] S.-F. Ge and H. Murayama, Apparent  $CPT$  violation in neutrino oscillation from dark non-standard interactions, [arXiv:1904.02518](https://arxiv.org/abs/1904.02518).
  - [14] P. B. Denton, A. Giarnetti, and D. Meloni, How to identify different new neutrino oscillation physics scenarios at DUNE, *J. High Energy Phys.* **02** (2023) 210.
  - [15] A. Gupta, D. Majumdar, and S. Prakash, Neutrino oscillation measurements with JUNO in the presence of scalar NSI, [arXiv:2306.07343](https://arxiv.org/abs/2306.07343).
  - [16] A. Medhi, D. Dutta, and M. M. Devi, Exploring the effects of scalar non standard interactions on the  $CP$  violation sensitivity at DUNE, *J. High Energy Phys.* **06** (2022) 129.
  - [17] A. Medhi, M. M. Devi, and D. Dutta, Imprints of scalar NSI on the  $CP$ -violation sensitivity using synergy among DUNE, T2HK and T2HKK, *J. High Energy Phys.* **01** (2023) 079.
  - [18] A. Medhi, A. Sarker, and M. M. Devi, Scalar NSI: A unique tool for constraining absolute neutrino masses via  $\nu$ -oscillations, [arXiv:2307.05348](https://arxiv.org/abs/2307.05348).

- [19] T. Sarkar, Probing non-unitarity of neutrino mixing in the scenario of Lorentz violation and dark nonstandard interaction, [arXiv:2209.10233](#).
- [20] D. K. Singha, R. Majhi, L. Panda, M. Ghosh, and R. Mohanta, Study of scalar non standard interaction at Protvino to Super-ORCA experiment, [arXiv:2308.10789](#).
- [21] A. Sarker, A. Medhi, D. Bezboruah, M. M. Devi, and D. Dutta, Impact of scalar NSI on the neutrino mass hierarchy sensitivity at DUNE, T2HK and T2HKK, [arXiv:2309.12249](#).
- [22] K. S. Babu, G. Chauhan, and P. S. Bhupal Dev, Neutrino nonstandard interactions via light scalars in the Earth, Sun, supernovae, and the early Universe, *Phys. Rev. D* **101**, 095029 (2020).
- [23] B. Dutta, S. Ghosh, K. J. Kelly, T. Li, A. Thompson, and A. Verma, Non-standard neutrino interactions mediated by a light scalar at DUNE, [arXiv:2401.02107](#).
- [24] B. Dutta, S. Ghosh, T. Li, A. Thompson, and A. Verma, Non-standard neutrino interactions in light mediator models at reactor experiments, *J. High Energy Phys.* **03** (2023) 163.
- [25] E. Aprile *et al.* (XENON Collaboration), Search for new physics in electronic recoil data from XENONnT, *Phys. Rev. Lett.* **129**, 161805 (2022).
- [26] S. K. A., A. Majumdar, D. K. Papoulias, H. Prajapati, and R. Srivastava, Implications of first LZ and XENONnT results: A comparative study of neutrino properties and light mediators, *Phys. Lett. B* **839**, 137742 (2023).
- [27] A. N. Khan, Light new physics and neutrino electromagnetic interactions in XENONnT, *Phys. Lett. B* **837**, 137650 (2023).
- [28] R. L. Workman *et al.* (Particle Data Group Collaboration), Review of particle physics, *Prog. Theor. Exp. Phys.* **2022**, 083C01 (2022).
- [29] P. Huber, M. Lindner, and W. Winter, Simulation of long-baseline neutrino oscillation experiments with GLOBES (General Long Baseline Experiment Simulator), *Comput. Phys. Commun.* **167**, 195 (2005).
- [30] P. Huber, J. Kopp, M. Lindner, M. Rolinec, and W. Winter, New features in the simulation of neutrino oscillation experiments with GLOBES 3.0: General Long Baseline Experiment Simulator, *Comput. Phys. Commun.* **177**, 432 (2007).
- [31] G. L. Fogli, E. Lisi, A. Marrone, D. Montanino, and A. Palazzo, Getting the most from the statistical analysis of solar neutrino oscillations, *Phys. Rev. D* **66**, 053010 (2002).
- [32] P. Huber, M. Lindner, and W. Winter, Superbeams versus neutrino factories, *Nucl. Phys.* **B645**, 3 (2002).